Design of Integrated Excitation Controller Based on Iterative Learning Control and Active Disturbance Rejection Control

Zheng Fan, Jingcai Bai, Junxiao Wu

Deparment of Automatic Control
Henan Institute of Technology
Xinxiang 453003, China

***Abstract* — Improving the stability of power systems and regulating the terminal voltage of generators are the two most important excitation control tasks. Improving the anti-interference ability of a power angle is an effective way to meet the adjustment of terminal voltage. The double closed-loop excitation controller was designed based on iterative learning control (ILC) and active disturbance rejection control (ADRC) to study multivariable output feedback control theory. The controller retained the ILC of the terminal voltage and added an inner-loop ADRC of a power angle. The ILC algorithm was adopted in the initial state and input of the outer-loop control of terminal voltage, which allowed certain initial repositioning errors to relax the requirement for the initial state. ADRC method was applied in the inner-loop control of a power angle to quickly eliminate the influence of disturbances on the system output variables. The designed controller was simulated and verified by an experiment for a three-machine power system. Simulation and experimental results confirm that the excitation controller can adapt to variations of the system network parameters, has strong robustness against internal and external disturbances, and can improve the dynamic stability of the system. The excitation controller also guarantees the adjustment precision of the terminal voltage.**

Keywords - ILC; ADRC; Multi-machine power system; Excitation controller

I. INTRODUCTION

The importance of synchronous generator excitation control in ensuring the stability of power systems has received increasing attention from scholars. Excitation control mainly regulates terminal voltage with high precision and restrains oscillation to improve the stability of a power system [1]. Maintaining generator terminal voltage is consistent with improving the transient and static stability of a power system against large and small disturbances. Regulating voltage can maintain constant terminal voltage but can produce negative damping effect, which is adverse to system dynamic stability [2]. A more effective measure is to increase the additional excitation control in the system, which has been researched for many studies. For example, AVR+PSS control mode [3] based on the PID control of terminal voltage adds PSS signal to the systems to provide positive damping and inhibit low-frequency oscillation; AVR+PSS is still used in most of China's units. However, PSS is designed for specific network models and low-frequency oscillation intervals. When the system condition is changed, the control effect is weakened, robustness and adaptability worsen, and PSS in a multi-machine system contains a number of parameters, which makes parameter regulation and optimization problems particularly difficult [4]. Additional excitation control methods, such as linear optimal excitation control [5, 6] and nonlinear control [7, 8], have been proposed. However, these methods either cannot meet the requirements on the regulation accuracy of the terminal voltage or solve the smooth nonlinear problem of a power system. Moreover, the additional excitation control parameters in the original calculation need to be revised, which limits its actual application. The main cause for the low regulation precision of terminal voltage is poor system damping capacity [2]; improving the anti-interference ability and robustness of power angle is effective to improve the regulation precision of terminal voltage. Active disturbance rejection control (ADRC) [9, 10] is a nonlinear robust control method with the advantages of small overshoot, fast convergence, high precision, strong anti-interference ability, and simple algorithm. Its uses of a nonlinear structure was proposed in recent years to fundamentally overcome the defects inherent in the classical PID (i.e., the error is not reasonable, differential and integral action need to be improved, and the linear combination mode of the error signal is not the most suitable). ADRC has become a hot research topic for many scholars in recent years, and many studies have been conducted on the application of ADRC to the excitation control of generators [11]. Iterative learning control (ILC) does not depend on the accurate mathematical model of plants and can learn the current control signal through previous information and measured tracking error. ILC has a simple structure, high tracking precision, and less prior knowledge; it can also adapt to a nonlinear strong coupling dynamic system with high uncertainty, which has been a wide concern in recent decades [12, 13].

Therefore, the double closed-loop integrated excitation controller based on ILC and ADRC, as well as E.J. Davison's robust regulator structure and the third-order nonlinear mathematical model of the synchronous generator, is formed to adjust the terminal voltage high precisely on the basis of strong damping. The outer-loop ILC of terminal voltage is added to the system based on the inner-loop ADRC of the power angle. The ILC algorithm is adopted

both in the initial state and the input value. The system gives overall consideration to the multiple tasks and goals of the excitation control system and does not focus on one point. The power system is interconnected by a number of synchronous generators, which interact among themselves. Compared with the single-machine infinite power system, more types of equipment in the multi-machine system are found, and the control is more complex. Hence, the integrated control of the multi-machine system is more practical and significant.

II. DESCRIPTION OF THE PROBLEM

When the equivalent damping windings of the d- and q-axis is neglected, the electromagnetic transient of the excitation winding f is only considered, and the input mechanical power is constant. Consider the i-th generator of an n-machine power system. Dynamic equation [8] can be expressed as

$$\begin{cases} \dot{\delta}_i = \omega_i - \omega_0 \\ \dot{\omega}_i = \dfrac{\omega_0}{H_i}(P_{mi} - P_{ei}) - \dfrac{D_i}{H_i}(\omega_i - \omega_0) + \eta_{i1} \\ \dot{E}'_{qi} = -\dfrac{1}{T'_{d0i}} E'_{qi} + \dfrac{1}{T'_{d0i}} U_{fi} + \eta_{i2} \end{cases} \tag{1}$$

The electrical parameters related to the system are

$$P_{ei} = U_{tdi} I_{di} + U_{tqi} I_{qi} = \left[E'_{qi} + \left(x_{qi} - x'_{di} \right) I_{di} \right] I_{qi}$$

$$I_{di} = -\sum_{j=1}^{n} E'_{qj} B_{ij} \cos \delta_{ij}$$

$$I_{qi} = \sum_{j=1}^{n} E'_{qj} B_{ij} \sin \delta_{ij}$$

$$U_{tdi} = x_{qi} I_{qi}$$

$$U_{tqi} = E_{qi} - x_{di} I_{di} = E'_{qi} - x'_{di} I_{di}$$

$$U_{ti} = \sqrt{U_{tdi}^2 + U_{tqi}^2}$$

The definitions of the above parameters are presented in [8].

The rest is per unit (pu), except for δ_i. ω_i, H_i and T'_{d0i}, which are rad, rad/s, and s, respectively.

Eq. (1) can be rewritten as the uncertain affine nonlinear system below:

$$\begin{cases} \dot{x}_i = f_i(x) + g_i(t) u_i + \eta_i \\ y_i = h_i(x) \end{cases} \tag{2}$$

Where the system state vectors are $x_i = \left[\delta_i, \omega_i, E'_{qi} \right]^T$; the input vectors are $u_i = U_{fi}$; y_i represents output, which can be selected flexibly; $g_i(t)$ represents the function matrix $\left[0, 0, \dfrac{1}{T'_{d0i}} \right]^T$;

$$f_i(x) = \left[\omega_i - \omega_0, \frac{\omega_0}{2H_i}(P_{mi} - P_{ei}) - \frac{D_i}{2H_i}(\omega_i - \omega_0), -\frac{E'_{qi}}{T'_{d0i}} \right]^T,$$

which is for the nonlinear function vector; and d_i represents the internal and external disturbances in the system.

III. DESIGN OF INTEGRATED EXCITATION CONTROLLER BASED ON ILC AND ADRC

Fig.1 shows a block diagram of the excitation control system, which is mainly composed of excitation regulator, power unit, synchronous generator, and measurement unit. In addition to the main circuit, a secondary circuit is introduced to the system, which can overcome the disturbance into the secondary circuit and improve the dynamic performance. The outer-loop main controller is in charge of the constant output of terminal voltage, and the output of the main controller is used as the input of the inner-loop secondary controller. Compared with the outer-loop controller, the inner-loop controller is mainly responsible for the strong damping control to power angle, and the control is more rapid and effective.

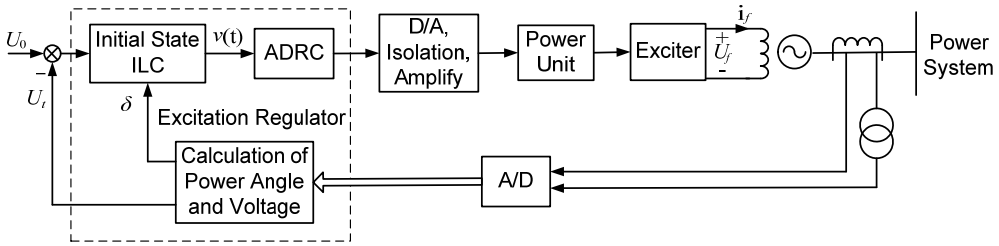

Figure 1. Block diagram of the control system

3.1 Design of outer-loop ILC of terminal voltage

One of the main functions of the excitation control system is to regulate the terminal voltage of the generator. Hence, the system output y_i can be selected as U_{ti} and compared with the reference value. The error is obtained, and the fixed value control is performed by the outer-loop main regulator. Open-loop PI-type ILC algorithm with initial state learning is selected as the control law. Figure 2 shows the algorithm structure. Open-loop ILC is one type of feed-forward control that can rapidly eliminate the oscillation caused by the delay of the error signal and reduce the impact of disturbance on the system by introducing feedback. The initial state also learns and allows a certain existing error to relax the requirement on initial state positioning. In open-loop PI-type ILC, initial state learning law can be expressed as

$$u_{k+1}(t) = u_k(t) + P_o e_k(t) + I_o \int_0^t e_k(\tau) d\tau \quad (3)$$

$$x_{k+1}(0) = x_k(0) + L e_k(0) \quad (4)$$

Where P_o, I_o, and L are the learning gain matrices of proportional, integral terms, and initial state learning law, respectively. $e_k(t) = y_d(t) - y_k(t)$, where $e_k(t)$ is the k-th tracking error of time t. $u_d(t)$ and $x_d(t)$ are the control and state vectors of the desired trajectory respectively.

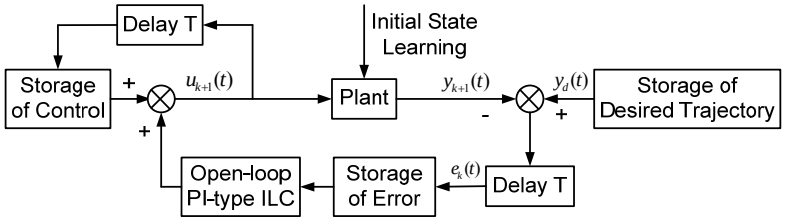

Figure 2. Structure of control system based on ILC with initial state learning

Assuming that the functions $f_i(x)$ and $g_i(t)$ are piecewise continuous in $t \in [0,T]$, and $h_i(x)$ has a partial derivative, Eq. (2) satisfies the following conditions.

Assumption 1. The function $f_i(x)$ is uniformly globally Lipschitz with respect to x, that is, a constant is $l_f > 0$, such that $x_1, x_2 \in R^n$. $\| f_i(x_1) - f_i(x_2) \| \le l_f (\|x_1 - x_2\|)$.

Assumption 2. For all x, $h_{ix}(x) = \dfrac{\partial h_i(x)}{\partial x} \neq 0$ and $h_i(x)$ are uniformly bounded and globally Lipschitz with respect to x.

Assumption 3. $\|\eta_{k+1} - \eta_k\| \le d_\eta$.

Assumption 4. The desired output trajectory $y_d(t)$ is continuous on $[0,T]$.

Assumption 5. The only expected input $u_d(t)$ exists, such that the corresponding state variables are $x_d(t)$, and the output is $y_d(t)$.

Assumption 6. The initial value of each iteration is different, and the k-th iteration initial value is $x_k(0)$.

The following notations are used to make the formula concise:

$$m_0 = \frac{1 - \mathrm{e}^{(l_f - \lambda)T}}{\lambda - l_f}$$

$$m_1 = \left[l_f P_o g_i + l_f I_0 \right] m_0$$

$$\delta x_{ik} = x_{ik+1} - x_{ik}$$

$$\xi_{ik} = x_{ik} + \gamma \delta x_{ik}, 0 \le \gamma \le 1$$

$$c_x = \sup_{t \in [0,T]} \left\| h_{ix}(\xi_{ik}) \right\|$$

$$\rho = 1 + c_x m_1$$

$$M_1 = c_x L$$

$$M_2 = c_x m_0$$

Theorem: For system (2), the iterative learning laws are given as (3) and (4), and all the parameters satisfy Assumptions 1 to 6. ρ exists, such that $\|e_{k+1}\|_\lambda \le \rho \|e_k\|_\lambda + M_1 \|e_k(0)\|_\lambda + M_2 \|d_\eta\|_\lambda$, $0 \le \rho < 1$. When the selected λ is large enough to make $0 \le M_1 < 1$ and $0 \le M_2 < 1$, for all $t \in [0,T]$, $\lim_{k \to \infty} \|e_k\|_\lambda = 0$, $\lim_{k \to \infty} y_k(t) = y_d(t)$.

3.2 Design of inner-loop ADRC of power angle

Adjusting the terminal voltage automatically can produce a negative damping effect while maintaining constant voltage. The main reason is the change of power angle that causes the change of terminal voltage and the inertia of the generator itself. Hence, the inner EMF's change delays the voltage's change. Therefore, an inner-loop ADRC of the power angle is added based on the outer-loop ILC of terminal voltage in this design and according to the double closed-loop control.

The structure of ADRC is composed of three parts [9]: tracking differentiator (TD), extended state observer (ESO), and nonlinear state error feedback control law (NLSEF). The structure is shown in Figure 3.

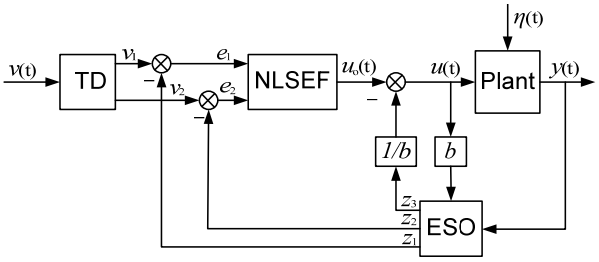

Figure 3. Structure of ADRC

For the plant of Eq. (1), if η_i satisfies the matching conditions of uncertainty, let

$$\begin{aligned} g_1 &= \delta_i \\ g_2 &= \omega_i - \omega_0 \\ g_3 &= \dot{\omega}_i \end{aligned} \tag{5}$$

Then, Eq. (1) can be written as

$$\begin{cases} \dot{g}_1 = g_2 \\ \dot{g}_2 = g_3 \\ \dot{g}_3 = f_0(x) + c_0(x)u + \eta \end{cases} \tag{6}$$

Where u is the control variable and excitation voltage, and η contains all the inside and outside disturbances, $y_i = h_i = g_1$.

3.2.1 TD

TD can track the given input signal with arbitrary precision. If the input signal is $v(t)$, then TD outputs tracking signal $v_1(t)$ and its differential signal $v_2(t)$, and the dynamic equation is

$$\begin{cases} \dot{v}_1 = v_2 \\ \dot{v}_2 = f_{st}(v_1 - v, v_2, r, h_0) \end{cases} \tag{7}$$

Where r is the speed factor, h_0 is the filter factor, and $f_{st}(\cdot)$ is the nonlinear function as follows:

$$f_{st}(x_1, x_2, r, h_0) = \begin{cases} -r(a/d), & |a| \le d \\ -r\,\mathrm{sgn}(a), & |a| > d \end{cases} \tag{8}$$

Where $a = \begin{cases} x_2 + \dfrac{a_0 - d}{2}\mathrm{sgn}(y), & |y| > d_0 \\ x_2 + \dfrac{y}{h_0}, & |y| \le d_0 \end{cases}$, $d = rh_0$, $d_0 = dh_0$, $a_0 = \sqrt{d^2 + 8r|y|}$, and $y = x_1 + h_0 x_2$.

3.2.2 ESO

The information in the input and output of the plant show that ESO can estimate the state variables of the system and the total disturbance in real time. z_1, z_2 and z_3 can track the outputs y, y', and y'', respectively. z_4 can estimate total disturbance. For the plant of Eq. (6), the fourth-order dynamic equation of ESO can be written as

$$\begin{cases} e = z_1 - y \\ \dot{z}_1 = z_2 - \beta_1 e \\ \dot{z}_2 = z_3 - \beta_2 f_{al}(e, a_1, \delta_0) \\ \dot{z}_3 = z_4 - \beta_3 f_{al}(e, a_2, \delta_0) + b_0 u \\ \dot{z}_4 = -\beta_4 f_{al}(e, a_3, \delta_0) \end{cases} \tag{9}$$

The nonlinear function $f_{al}(\cdot)$ is defined as follows:

$$f_{al}(e_0, a, \delta) = \begin{cases} \dfrac{e_0}{\delta^{1-a}}, & |e_0| \le \delta \\ |e_0|^a \mathrm{sgn}(e_0), & |e_0| > \delta \end{cases} \tag{10}$$

Where a_1, a_2, a_3 are the nonlinear factors; $\beta_1, \beta_2, \beta_3, \beta_4$ are the error compensation gains; and δ_0 is the filter factor.

3.2.3 NLSEF

The outputs v_1, v_2 of TD are compared with the state estimates z_1, z_2 given by ESO. The errors are e_p, e_d, which generate u_0 with a certain nonlinear combination form and combine with the estimate z_3 to form the control variable u. The corresponding expressions are

$$u = u_0 - \frac{z_3}{b_0},\ e_p = v_1 - z_1,\ e_d = v_2 - z_2, \text{ and}$$

$$u_0 = k_p f_{al}(e_p, a_4, \delta_1) + k_d f_{al}(e_d, a_5, \delta_1)$$

Where u is the excitation voltage U_{fi}, k_p and k_d are the proportional and differential gain respectively, a_4 and a_5 are the nonlinear factors, and δ_1 is the filter factor. The appropriate selection of these parameters can construct control input u_0.

3.2.4 Parameter selection of ADRC

Parameters in ADRC can be selected according to "the separation principle," that is, TD, ESO, and NLSEF are regarded as three separate parts.

First, the parameters of TD and ESO are selected until satisfactory results are obtained, and the total parameters of the controller are adjusted with NLSEF.

The parameters of ADRC in this system mainly include r, h_0 of TD; $a_1, a_2, a_3, \beta_1, \beta_2, \beta_3, \beta_4, \delta_0$ of ESO; and $k_p, k_d, a_4, a_5, \delta_1, b_0$ of NLSEF.

After the integral step h is determined, the selection of speed factor r is related to the length of the system transient process and performance. The filter factor can only meet $h_0 \le h$. Let $h_0 = h$ to reduce the difficulty of parameter selection. Let $a_1, a_2, a_3 \in [0,1]$, the smaller the value, the stronger the ability to adapt to internal and external disturbances. The feedback coefficient should satisfy the condition $\beta_1 \le \beta_2 \le \beta_3 \le \beta_4$, but the latter value β should not become large, otherwise, the observation effect is not good. δ that is excessively large or small affects the accuracy of estimate value, takes 0.1, and fine tunes. The nonlinear factors of NLSEF are generally selected as $a_4 = 0.5$ and $a_5 = 1.5$. k_p and k_d can be adjusted according to the PID parameter tuning method.

IV. NUMERICAL SIMULATION

The sampling step size is 0.001 in the simulation process. The parameters of TD in the inner-loop ADRC controller are $r = 100$ and $h_0 = 0.001$. $a_1 = 0.75$, $a_2 = 0.5$, $a_3 = 0.25$, $\beta_1 = 10$, $\beta_2 = 200$, $\beta_3 = 650$, $\beta_4 = 1100$, and $\delta_0 = 0.12$ are selected in ESO, $a_4 = 0.5$, $a_5 = 1.5$, $k_p = 6$, and $k_d = 31$ in NLSEF, and $P_o = 12$, $I_o = 7$ and $L = 9.5$ in outer-loop ILC.

The three-machine power system is shown in Figure 4. To verify the performance of the integrated excitation controller based on ILC and ADRC, the controller is compared with the conventional AVR+PSS. The open-loop ILC excitation controller based on terminal voltage deviation and simulations are performed. The generator G3 is a balancing machine, which is represented by an infinite bus. The relevant parameters of the simulation model are described in literature [14]. During simulation, the input mechanical power remains constant, and the initial operation conditions of the system are selected as δ_{10}=26.0^0 , $P_{m10}=0.65$ pu , $U_{10}=1.03$ pu , δ_{20}=52^0 , $P_{m20}=0.8$ pu , $U_{20}=1.0$ pu , $U_{30}=1.0$ pu , and ω_0=314.16 rad/s . For the i-th generator, let $P_{ei}\in(0.3,1.2)$ pu , $B_{ii}\approx B_{ii0}$, $U_{fi0}=1.0$ pu , and $|U_{fi}|\le 4$ pu , where $i=1,2$. Subscript 0 denotes the initial value.

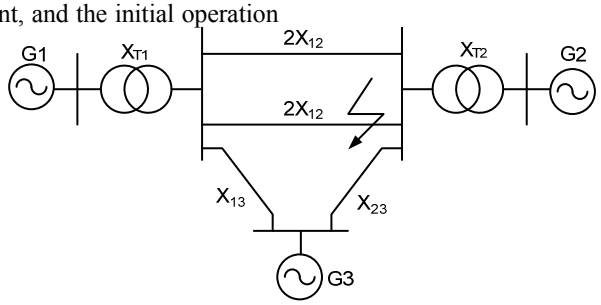

Figure 4. Three-machine power system

The system starts running from the equilibrium state. The three-phase grounding short-circuit fault in the simulation occurs at the first end of the transmission lines between generators G1 and G2 at t=1 s and t=1.15 s respectively. The faulted line is isolated from the healthy system, and another line protective action trips.

Figures 5 and 6 show the terminal voltage curves and power angle curves respectively under the controls of the three types of excitation controllers. The solid line denotes the use of double closed-loop integrated excitation controller based on ILC and ADRC, the dashed line denotes the use of open-loop ILC, and the dotted line represents the use of AVR+PSS.

Figure 5 indicates that the terminal voltages of the system can settle down to a new steady state after a certain time under the three types of controllers. The terminal voltage response passes through a short transient process and ends at t=1.4 s under the integrated excitation controller. The voltage is basically the same as the initial value, which makes the adjustment precision high. However, under the open-loop ILC and AVR+PSS, the waveform oscillates more severely and takes a longer time to end the transient process.

Figure 6 shows that, under the controller designed above, the oscillation amplitude is small, the convergence speed is fast, and the power angel output can return to the initial steady state. Hence, the designed system has strong damping capacity and can better maintain the power angle.

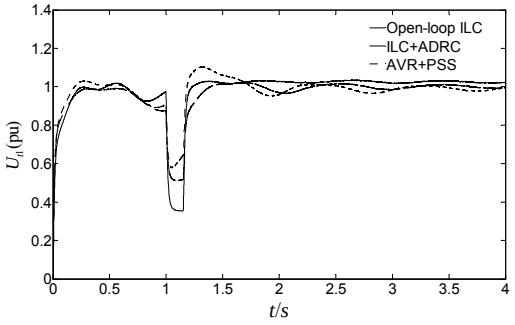

(a) Terminal voltage curves of G1

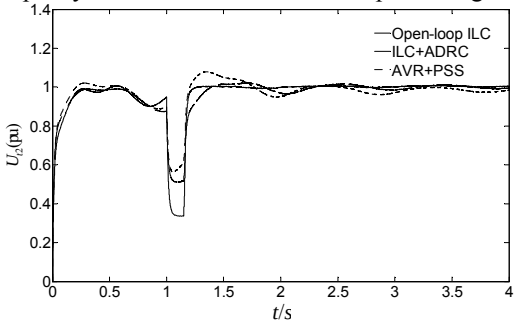

(b) Terminal voltage curves of G2

Figure 5. Terminal voltage curves of the generators

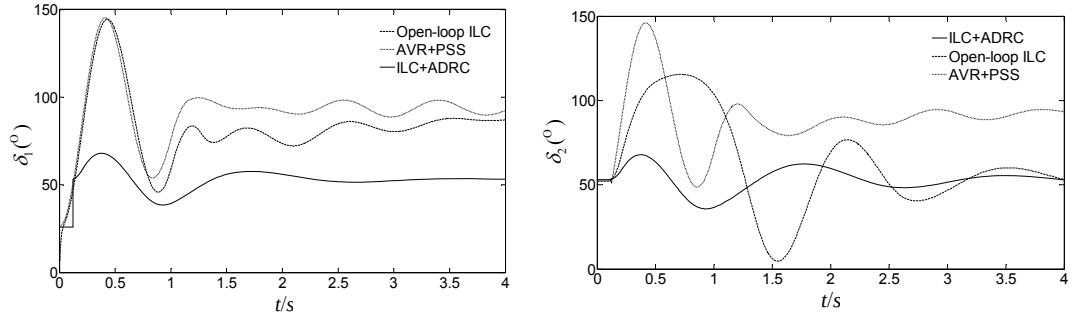

(a) Power angle curves of G1 (b) Power angle curves of G2

Figure 6. Power angle curves of the generators

V. DYNAMIC MODEL EXPERIMENT ANALYSIS

The excitation controller is tested by two sets of units composed of 3 kW DC motor and 2 kW synchronous generator to verify the feasibility and effectiveness of the excitation controller designed in this paper. An experiment platform based on TMS320F2812 is also developed to carry out the most serious three-phase short-circuit test in the power system and automation laboratory co-established by the institute and the XJ Group Corporation.

5.1 Experiment platform

The experiment platform is mainly composed of a control panel, a driving device, an exciter, two DC motors, and a three-phase AC synchronous generator, as shown in Figure 7. The DC motor acts as the prime mover; the excitation regulator takes the TMS320F2812 as the control core, which has a strong event management and embedded control capability with 32-bit fixed-point CPU. It is especially suitable for occasions where a large number of data needs to be processed [15]. The main frequency is 150 MHz. The data calculation and processing ability can fully satisfy the requirement on control response time in the excitation control system.

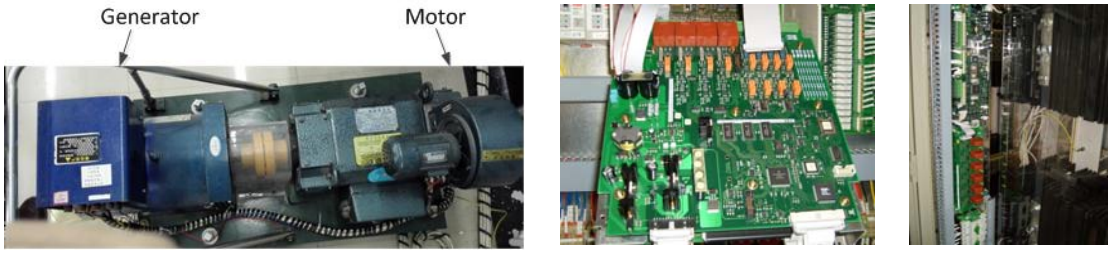

(a) Generator unit (b) Control panel (c) Driving device

Figure 7. Experiment platform

5.2 System structure and parameters

The system structure is shown in Figure 4.

Parameters used in the circuit: Dual transmission lines are used between generators G1 and G2. The resistance of each line is 11.5 Ω. The corresponding per-unit value is 0.55, $x_{13} = 0.42$, and $x_{23} = 0.53$.

Transformer parameters: Transformation ratios of the two step-up transformers are both 400/800.

The prime movers are three pairs of poles brushless DC motors. The rated power corresponding to G1 is 3 kW, and the rated speed is 1500 r/min. The rated power corresponding to G2 is 5 kW, and the rated speed is 2500 r/min.

Parameters of G1: The rated power is 2 kW, the rated voltage is 400 V, the rated current is 3.6 A, the rated excitation voltage is 56 V, and the rated excitation current is 2.5 A.

Parameters of G2: The rated power is 3 kW, the rated voltage is 400 V, the rated current is 5.4 A, the rated excitation voltage is 70 V, and the rated excitation current is 3 A.

5.3 Dynamic model experiment results and analysis

During testing, the two DC motors are tested first to make them run stably at a rated speed. The excitation current is adjusted to make the generator work at the rated state. In one transmission line near G2, three-phase line-to-ground fault occurs and continues for 0.2 s. The fault line trips out after another 0.2 s. During the experiment, the control method designed above is compared with the conventional AVR+PSS, and the results are shown in Figures 8–11.

Figures 8 and 9 show the rotor speed curves and power angle curves of G2 relative to G1. Figure 9 shows that both control methods increase the power angle difference between two generators when it reaches a new steady state. However, the excitation controller designed above can make the relative movement return to a new rest in a relatively short

time compared with the conventional AVR+PSS. The designed controller has a stronger damping capacity to make the system return more quickly to the power angle steady state and effectively improve the dynamic stability of the system.

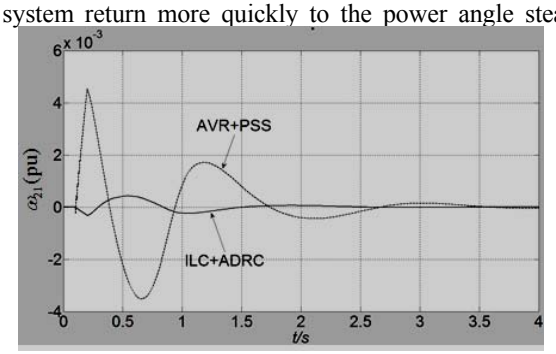

Figure 8. Rotor speed difference curve between G2 and G1

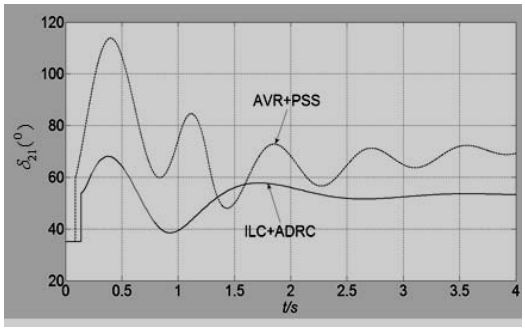

Figure 9. Power angle difference curve between G2 and G1

Figures 10 and 11 show the terminal voltage curves and active power response curves of G1. The overshoot and settling time of terminal voltage under the control of ILC+ADRC are 13.2% and 1.2 s respectively. However, the overshoot and settling time under the control of AVR+PSS are 29% and 2.74 s respectively. Therefore, the stability of the system and the regulation accuracy of terminal voltage are high under the control of ILC+ADRC. Moreover, although active power has a violent oscillation when the fault occurs, the amplitude becomes smaller after the second swing, and the oscillation is quickly suppressed. Hence, the overall control effects indicate that ILC+ADRC controller is superior to the conventional AVR+PSS.

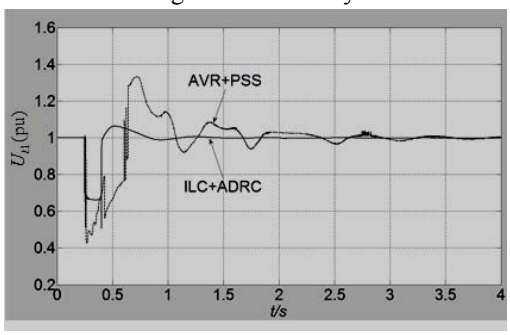

Figure 10. Terminal voltage curves of G1

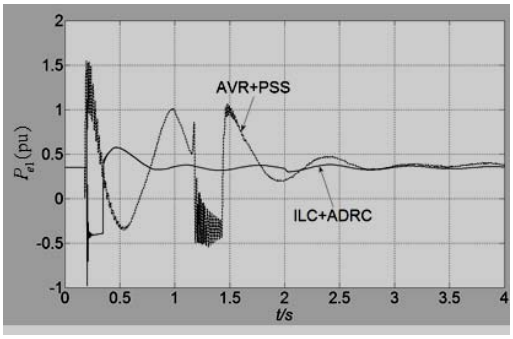

Figure 11. Active power curves of G1

VI. CONCLUSION

Improving the anti-interference ability of the power angle can increase the system dynamic stability and effectively improve the regulation accuracy of the terminal voltage to achieve the two most important excitation control tasks. The double closed-loop integrated excitation control system for a three-machine power system is constituted according to the addition of the inner-loop ADRC of power angle based on the outer-loop ILC of terminal voltage. The system can fully use the advantages of double closed-loop control, and the two types of control methods can complement each other. The ADRC used in the inner loop can quickly eliminate most of the interference to reduce the impact on the system output. The open-loop PI-type ILC algorithm with initial state learning used in the outer loop can relax the requirements on the initial positioning, reduce the number of iterations, and enhance the convergence rate. The regulation accuracy of terminal voltage is ensured given that system dynamic stability is improved. The system designed in this paper is verified by simulation and experiment. Results show that when the system structure and parameters are changed, the excitation control mode compared with open-loop ILC and conventional AVR+PSS can bear greater interference, has stronger robustness, and can meet the regulation accuracy of terminal voltage.

This paper studied the three-machine power system. The control strategy will be considered for application to other systems. The optimization of parameters in ILC and ADRC should also be considered for further research.

REFERENCES

[1] Cheng Q.M., Cheng Y.M., Xue Y., Hu X.Q., "Development and prospects of excitation control methods for synchronous generator", Electric Power Automation Equipment, vol. 32, No.5, pp.108-117, 2012.
[2] Liu Q., "Power system stability and generator excitation control", Beijing: China Electric Power Press, pp. 103-130,2007.
[3] Touil S, Attous DB, "Effect of different membership functions on fuzzy power system stabilizer for synchronous machine connected to infinite bus", International Journal of Computer Applications, vol. 71, No.7, pp. 20-26, 2013.
[4] Kundur P., "Power system stability and control", New York: McGraw-Hill, pp. 766–770, 1994.

[5] Leon A.E., Mauricio J.M., Solsona J.A., "Multi-machine power system stability improvement using an observer-based nonlinear controller", Electric Power Systems Research, vol. 89, pp. 204-214, 2012.
[6] Ma J., Wang H.J., Zhang P., "Renewed investigation on power system stabilizer design", Science China Technological Sciences, vol. 54, No.10, pp. 2687-2693,2011.
[7] Yuan R.X, Ruan Y., Hu P., "Nonlinear excitation controller design for power systems: an I&I approach", Journal of Control Theory and Applications, vol. 10, No.4, pp. 554-558, 2012.
[8] Ruan Y., Yuan R.X., Wan L., Zhao H.S., "Nonlinear robust voltage control for synchronous generators", Transactions of China Electrotechnical Society, vol. 27, No.9, pp. 9-16, 2012.
[9] Guo B.Z., Zhao Z.L., "On convergence of the nonlinear active disturbance rejection control for MIMO systems", SIAM J on Control and Optimization, vol. 51, No.2, pp.1727-1757, 2013.
[10] Zhang C.L., Yang J., Li S.H., Yang N., "A generalized active disturbance rejection control method for nonlinear uncertain systems subject to additive disturbance", Nonlinear Dynamics, vol. 83, No.4, pp.2361-2372, 2016.
[11] Li T.Y., Li H.M., Yu X.L., He Y., "Optimal Robust Sliding Mode Excitation Controller for Multi-machine power System", Proceedings of the CSU-EPSA, vol. 25, No.6, pp.87-92, 2013.
[12] Fujimori Atsushi, Ohara Shinsuke, "Parameter identification of continuous-time systems using iterative learning control", International Journal of Control, Automation and Systems, vol. 9, No.2, pp.203-210, 2011.
[13] Zhang C.L., Li J.M., "Adaptive iterative learning control of non-uniform trajectory tracking for strict feedback nonlinear time-varying systems", International Journal of Automation and Computing, vol. 11, No.6, pp.621-626,2014.
[14] Yan R., Dong Z.Y., Saha T.K., "A power system nonlinear adaptive decentralized controller design", Automatica, vol. 46, No.2, pp.330-336,2010.
[15] Karaarslan A., Iskende I., "A DSP based power factor correction converter to reduce total harmonic distortion of input current for improvement of power quality", Electrical Engineering, vol. 93, No.4, pp. 247-257, 2011.